Applied Water Science (2021) 11:95
https://doi.org/10.1007/s13201-021-01421-5

REVIEW ARTICLE

Heavy metals adsorption from contaminated water using moringa seeds/ olive pomace byproducts

Ibrahim Hegazy[1] · Mohamed E. A. Ali[2] · Ehab H. Zaghlool[2] · Ragaa Elsheikh[3]

Received: 14 January 2021 / Accepted: 4 May 2021 / Published online: 23 May 2021

Abstract

Several approaches have been used to reduce the accumulation of heavy metals in aqueous solutions, including adsorption to the surface of agricultural waste. Batch studies have been performed in this study to explore the adsorption of Fe^{2+}, Mn^{2+} on olive pomace (OP), and moringa seed husk (MSH). Fourier transform infrared and scanning electron microscopy also characterized the prepared adsorbent. Batch adsorption studies were performed, and the effects of adsorbent chemical structure, adsorbent dosage, pH, contact time, and initial ion concentration were investigated on Fe and Mn ions sorption and mechanism in order to maximize the removal efficiency of Fe and Mn. It was shown that the removal percentage of Fe^{2+} and Mn^{2+} were 83% and 91%, respectively, at optimum pH 5 and optimum time of 120 min at 5 g of OP. Although the removal percentage of Fe^{2+} and Mn^{2+} were 80.5% and 93%, respectively, at 5 g of MSH. The pseudo-second-order model was followed by the adsorption kinetics of Fe^{2+} and Mn^{2+} on OP and MSH, and the Langmuir model worked well with the adsorption isotherms. Based on their adsorption/desorption processes, OP and MSH adsorbents may be regenerated by DI water more than five times. The overall adsorption power of the OP adsorbent for Fe^{2+} and Mn^{2+} was 10.406 and 10.460 mg/g, and the MSH was 10.28 and 11.641 mg/g for Fe^{2+} and Mn^{2+}, respectively.

Keywords Moringa seeds husks · Olive pomace · Heavy metal removal · Adsorption isotherms · Reusability

Introduction

One of the main causes of water degradation of marine heavy metals is agricultural wastewater effluent. Aqueous toxic waste induces heavy metal pollution from many operations, such as metal plating, logging, tanning, etc. (Nieto et al. 2010). There are, however, several distinct strategies for extracting heavy metals from polluted water (Ince and Ince 2017). The key topics associated with low-cost adsorbents and their derivatives for use in the removal of contaminants from waste water were listed (Veglio and Beolchini 1997; Volesky 2001). Agricultural waste, municipal solid waste, biomass, clay minerals, and zeolites were included. It is apparent that inexpensive adsorbents have shown excellent pollutant-removal capabilities. Modifications of cheap adsorbents can modify their original properties, making them highly suited to the sorting of different kinds of waste materials (Sadegh et al. 2017). An immense amount of waste that is disrupted by the high content of organic carbon (cellulose, hemicellulose, lignin and polyphenols) is created by the olive oil industry (Martín-Lara et al. 2009). A number of these olive oil wastes have recently been tested with positive findings as heavy metal biosorbents (Gharaibeh et al. 1999; Martín-Lara et al. 2008). Nieto et al. (2010) examined the adsorption of Fe by olive stones in agricultural wastewaters. The percentage of iron adsorption increased from 30 to 70% when the initial biomass concentration rose from 25 to 125 g dm^{-3}. Moringa Oliefera Seeds Husks (MSH) have been used as an adsorbent to get rid of iron and manganese ions from the aqueous solution (Ghafar et al. 2017), Moringa oleifera seed powder has been researched. Ongulu (2015) investigated Moringa oleifera seed powder with a view of using it as a low-cost

✉ Ibrahim Hegazy
hemahegazy087@gmail.com

✉ Mohamed E. A. Ali
m7983ali@gmail.com

[1] The Holding Co for drinking water in Greater Cairo (10th of Ramadan Authority), Cairo, Egypt

[2] Hydrogeochemistry Department, Desert Research Center, Cairo 11753, Egypt

[3] Chemistry Department, Zagazig University, Cairo, Egypt

biosorbent for the removal of toxic heavy metals from wastewater. MOH was chemically activated using citric acid in order to improve the ability of adsorption. The adsorption analysis was carried out in the water bath shaker using the batch technique to explore various parameters; adsorbent dose (10 g/L), initial metal concentration (50 mg/L), contact time (90 min), at steady 100 rpm agitation. This study was performed to investigate the adsorption performance of environmental eco-friendly wastes, namely OP and MSH for the removal of Fe and Mn from aqueous solutions in the heavily populated study region, surrounded by sources of contamination or close to it and compare the efficiency of the two adsorbent materials. Nieto et al. (2010) used olive stones directly and characterized by mercuric porosimetry. The equilibrium adsorption capacity was higher when the particles size (from < 1 to 4.8 mm) decreased. The percentage of iron adsorption increased from 30 to 70% when the initial concentration of biomass increased from 25 to 125 g dm^{-3}.The optimum concentration of olive stones was fixed at 37.5 g dm^{-3}. The adsorption of iron was determined as a function of their initial concentration and multiplayer formed at high iron concentration. Fiol et al. (2006) reached that the highest value of Langmuir maximum uptake, (q_{max}), was found for cadmium (6.88×10^{-5} mol g^{-1}) followed by lead (4.47×10^{-5} mol g^{-1}), nickel (3.63×10^{-5} mol g^{-1}), and copper (3.19×10^{-5} mol g^{-1}) onto olive stone waste. Similar Freundlich empirical constants, k, were obtained for all metals (2.4×10^{-5} to 2.8×10^{-5}). Elouear et al. (2009) showed the equilibrium in the adsorption of Pb(II) and Zn(II) on exhausted olive pomace ash within 2 h of contact between the fly ash and the aqueous solution. Monolayer sorption capacities of EOPA were 8.76 and 7.75 mg g−1 for lead and zinc ions, respectively. Ali and Seng (2018) used Moringa oleifera press cake (MOPC) to remove the heavy metal from wastewater. The MOPC removed 69.99% Fe, 88.86% Cu, and 93.73% Cr at optimum concentration of 10,000 ppm, 5000 ppm, and 15,000 ppm, respectively. Aziz et al. (2016a, b) demonstrates that Moringa seeds, banana peel and their combination have the potential to be used as a natural alternative to the other water treatment agents for removing the Pb, Ni, and Cd from drinking water. Results showed that combined biomasses was able to met the Pb, Ni, and Cd WHO standards from higher Pb, Ni, and Cd initial concentrations which were up to 40 µg/L, 50 µg/L, 9 µg/L, respectively, compared to individual biomass of Moringa seed and banana peel.

Material and methods

Preparation of adsorbent materials.

Preparation of olive pomace adsorbent

From Ras Sidr, South Sinai, Egypt, the olive pomace solid waste was collected. An electric mixer grounded the olive pomace, removed large particles by a sieve with 4.75 diameter and obtained uniform sizes. OP was washed by boiled deionized water (on Jar test equipment for 90 min. at 200 rpm for 5 times) to remove the remaining organic matter which could interfere in the results (Nieto et al. 2010**).** They were dried in the oven for 3 h at 105°c and then placed in a jar for experimental work as shown in Fig. 1 a, b, and c.

Preparation of moringa seeds husks adsorbent

Moringa seeds were purchased from a local market.The husks were removed manually from the seeds and washed several times with boiled distilled water to remove all the dirt and other undesirable particulate matter. Then, it was dried in drying oven (JP Selecta Model DiGitHeat 19L/2,001,241) at 100 °C until constant weight is obtained. The dried MSH was ground using electrical grinder (Model Braun 850 W made in Germany) to achieve fine and uniform particles as in Fig. 1 d, e, and f.

Characterization

Surface images of nanoparticles were recorded using Quanta FEG 250 scanning electron microscope (FEI Company, USA) available at EDRC, DRC, Cairo. Samples were mounted onto SEM stubs. Applied SEM conditions were as follows: a 10.1 mm working distance, with in-lens detector with an excitation voltage of 20 kV.

Preparation of Fe^{2+} and Mn^{2+} adsorbate

By dissolving 7,0025 g of ferrous ammonium sulfate and 2,8727 g of potassium permanganate, the stock solutions (1000 mg / l) of Fe^{2+} and Mn^{2+} were prepared and the solution was stored in a volumetric flask at one liter mark. To achieve the correct concentration, the stock solution was diluted with double distilled water, varying from 10 to 1000 mg/l, as required for the experiments. Iron (510 nm) concentration and manganese (525 nm) concentration were calculated using the JP Selecta uv/visible

Fig. 1 preparation of **a** olive pomace adsorbent material **b** Moringa seeds Husks adsorbent material

Spectrophotometer phenonthroline and persulphate process, respectively (Standard Methods 2012).

Batch adsorption studies

Sorption tests were conducted at 100 rpm (Aziz et al. 2016a; b) by batch technique on jar test equipment (Model Flocumatic, J.P selecta, Spain). To elucidate the influence of certain parameters on the sorption of iron and manganese into OP and MSH, batch tests were administered. Those parameters investigated included pH, adsorbent dosage, concentration of metal ions, and contact time. All adsorption tests were conducted at pH 5, with HCl (1 N) and NaOH (1 N) solutions being modified. Both adsorption tests were performed in a 500 mL solution with a metal ion concentration of 50 ppm. Batch tests were conducted for various metal concentrations (10–300 mg/L), contact time (120 min), adsorbent dosage (0.5–7 g) and pH (2–7) in order to establish the optimal experimental conditions. The initial and final iron and manganese concentrations were calculated using a spectrophotometer (Model JP Selecta uv / visible). The amount of the metal adsorbed (% removal) by the sorbent was calculated using

$$\%\ \text{Removal Efficiency} = ((C_i - C_f)/C_i) \times 100 \quad (1)$$

The amount of adsorbed metal ions onto the surface of the adsorbent was calculated from the mass balance expression given by:

$$q_e = \frac{(C_i - C_f)}{\mathrm{M}} V, \quad (2)$$

where q_e is the amount of metal ions adsorbed (mg/g); C_i initial metal ion concentration (mg/L), C_f is the final metal ion concentration (mg/L), M is the mass of the adsorbent in (g), and V is the volume (liter) of the metal solution in contact with the adsorbent.

Adsorption isotherms

The adsorption isotherm models of Langmuir (1918) and Freundlich (1906) were used. For Langmuir model the linear form could be expressed from the following equation:

$$C_e/\,q_e = 1/\,K_L q_{max} + C_e/\,q_{max} \quad (3)$$

The Freundlich model, the linear form could be expressed from the following equation:

$$Log\, q_e = log\, k_F + (1/n)\, log\, C_e, \quad (4)$$

where C_e is the equilibrium concentration of Fe^{2+} and Mn^{2+} in mg/l, q_e and q_m are the adsorption amount at equilibrium (mg/g) and adsorption capacity (mg/g), respectively, and K_L is the Langmuir constant (L/mg). The values of K_L and qm can be obtained from the intercept and slope of C_e/q_e versus C_e (Fig. 10a and b). K_F is the empirical Freundlich constant (mg/g) and 1/n is the Freundlich exponent.

Adsorption kinetics

The pseudo-first-order kinetic model (Lagergren 1898) and pseudo-second-order kinetic model (Ys et al. 1999) were employed to fit the experimental data and to understand the adsorption mechanism of Fe^{2+} and Mn^{2+} ions using OP and MSH adsorbents. The equation of Pseudo-first-order kinetic model is as follows:

$$\text{Log}\left(q_e - q_t\right) = \log q_e - \left(\left(k_1/2.303\right) * t\right), \quad (5)$$

where q_t and q_e (mg /g) are the amounts of metal ions adsorbed per unit mass of the adsorbent at time t (min) and equilibrium, respectively, and k_1 (1/min) is the pseudo-first-order rate constant of the sorption process. The equation of Pseudo-second-order kinetic model is as follows:

$$t/q_t = 1/k_2 q_e^2 + t/q_e, \quad (6)$$

where k_2 [g/ (mg min)] is the pseudo-second-order rate constant.

Results and discussion

Characterization of OP and MSH

Olive pomace

Olive pomace is a sticky waste and polyphenolic compounds; in addition, it contains uronic acids, cellulose and lignin (Saviozzi et al. 2001). This complex matrix comprises numerous fixed polyvalent functional groups (such as carboxy, hydroxy, and methoxy groups) and a large number of fixed anionic and cationic functional groups that cause various mechanisms in solutions to bind metal ions: complexation, chelation, physical sorption, ion exchange, and electrostatic. Veglio and Beolchini (1997). In the adsorption mechanism where the biomass arrangement and some cavities on the external surface are porous in Fig. 2a, the morphology of fresh OP plays an avital role, which increases its overall surface area and thus easily increases the propensity of agglomeration between biomass and Fe^{2+} ions and Mn^{2+} ions, as shown in Fig. 2b and c, respectively (Bayramoğlu et al. 2006; Tsai et al. 2008; Nieto et al. 2010). As seen in Fig. 3a, the Fourier Transform Infrared (FTIR) spectra of fresh OP show large wide bands assigned to the surface hydroxyl group of about 3300 cm^{-1}. C = O, C = C alkene and C-O, respectively, are responsible for the peaks at 2362.21 cm^{-1}, 1635 cm^{-1} and 1030 cm^{-1}. Following the adsorption of Fe^{2+} metal ions, shown in Fig. 3b, the wavenumbers of fresh OP changed from 3300, 1635, and 1030 cm^{-1} to 3277.88, 1615, and 1029.94 cm^{-1}, respectively. On the other hand, after Mn^{2+} adsorption, the wavenumbers of new OP changed to 3279.16, 1616.85, and 1050.97 cm^{-1}, respectively, seen in Fig. 3c. It was concluded that OP may include various mechanisms such as ion exchange, electrostatic attraction and complexation, according to FTIR analysis study before and after adsorption (Hawari et al. 2014).

Moringa seeds husks

Various amino acids, vitamins, carbohydrates, glucosinolates, and fatty acid phenolics, which are functional groups capable of metal adsorption, are found in the MSH. It is a possible source of low-price adsorbent output due to the composition of MSH and its availability Ghafar et al. (2017). The MSH micrographs (Fig. 4a) indicate mesoporous structures of different pore sizes. Because of the available binding cavities for the metal ions, these surface properties will result in high metal binding (Maina 2016). Figure 4b shows the wavenumbers of fresh MSH, which was changed from 3333, 1654.7, and 1029.76 cm^{-1} to 3323.42, 1646.89, and 1030.12 cm^{-1}, respectively. On the other hand, the wavenumbers of new MSH shifted to 3327, 1636.3, and 1052.08 cm^{-1}, respectively, after Mn^{2+} uptake seen in Fig. 4c. As seen in Fig. 5b and c, the decrease in amplitude and change of the above-mentioned peaks may be attributed to the relationship between the metal and the specific functional groups. The hydroxyl (OH) groups, C–H, C = C of alkenes, and C–O of carboxylic acids are the functional groups responsible for metal removal in MSH (Demirbas et al. 2004; Rahman and Islam 2009).

Factors affecting on removal of Fe^{2+}, Mn^{2+} ions

Effect of initial pH

Figure 6 shows the role of the solution pH value (2 to 7) on the metal adsorption on OP and MSH. The figure reveals that the ideal pH for adsorption of ions is 5. For OP, $Fe^{2+}$and Mn^{2+} removal efficiency improved dramatically from 8 and 5 percent (at pH 2) to 89 percent and 79 percent (at pH 5), respectively, for $Fe^{2+}$and Mn^{2+}. On the other hand, for $Fe^{2+}$and Mn^{2+}, MSH indicates a higher removal efficiency that has improved from 12 and 3.5 percent (pH 2) to 93 and 82 percent (pH 5). There is a competition between hydrogen ions and metal ions at a lower pH for a small number of binding sites, which will minimize $Fe^{2+}$and Mn^{2+} sorption. Whereas, as the number of hydrogen ions decreased and the O.P, MSH adsorbents allowed more ligands to form complexes with $Fe^{2+}$and Mn^{2+} at higher pH values, leading to sorption of $Fe^{2+}$and Mn^{2+} (Tan et al. 2015; Blázquez et al. 2005).

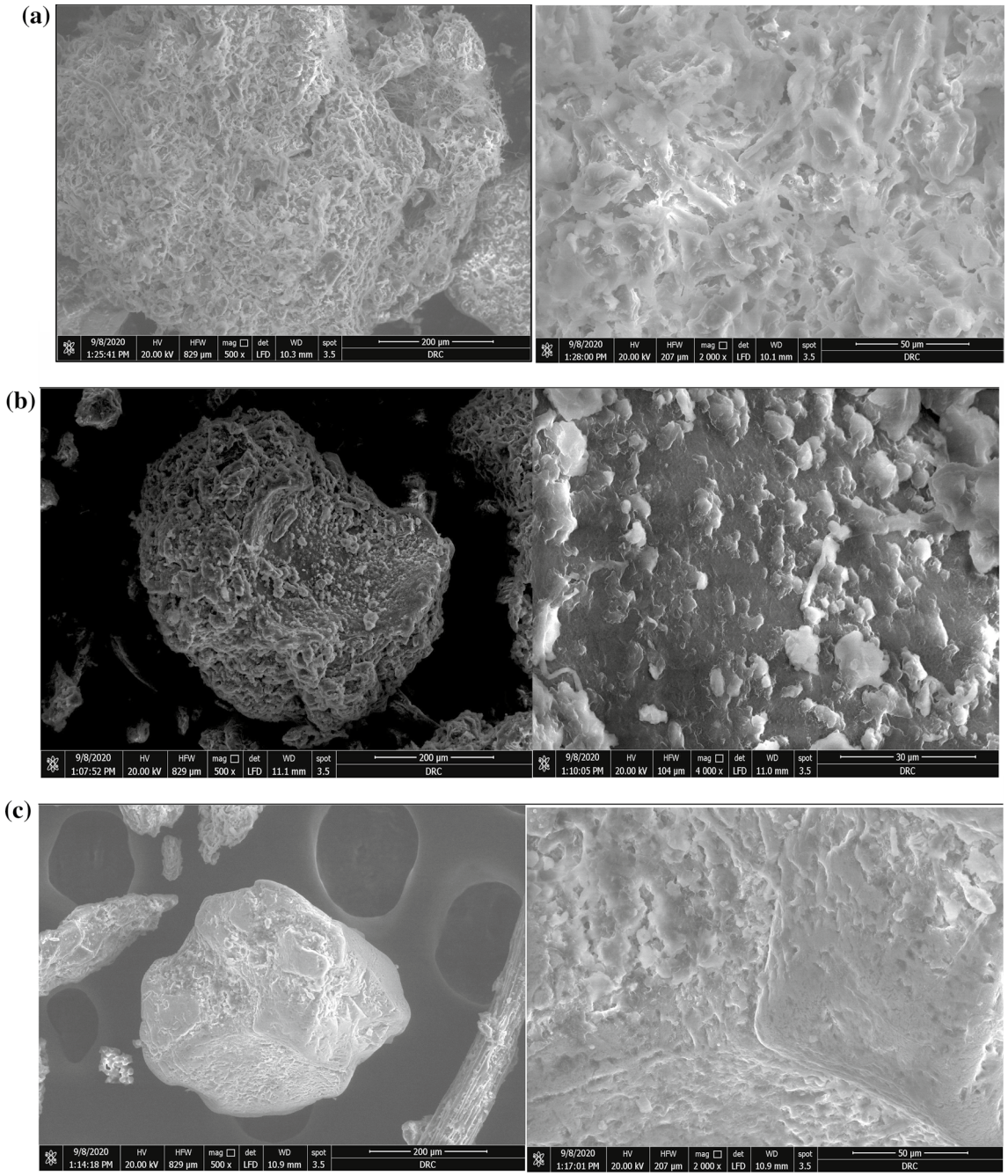

Fig. 2 SEM image of OP before adsorption (**a**) OP after Fe^{2+} adsorption (**b**) OP after Mn^{2+} adsorption(**c**) at two magnifications

Effect of adsorbent dosage

The dependence of Fe^{2+} and Mn^{2+}adsorption on the biomass of OP and MSH was examined at pH 5 by changing the biosorbent dose for each Fe^{2+} and Mn^{2+} in 500 ml of 50 mg/l solution from 0.5 to 7.0 g for OP and MSH. Figure 7 indicates that the removal efficiency improved from 10.4 to 52% for $Fe^{2+}$and Mn^{2+}, respectively, to 87% and 82% in the case of OP. On the other hand, the removal efficiency improved from 24 to 26% for $Fe^{2+}$and $Mn^{2+}$to 96% and 98% for $Fe^{2+}$and Mn^{2+}, respectively, by using MSH. The increased adsorbent dose would improve the surface area that can be used for sorption (Ponnusami et al. 2007; Cengeloglu et al. 2007; Bouguerra et al. 2008). For every Fe^{2+} and Mn^{2+}, the chosen dose of OP and MSH was 5 g.

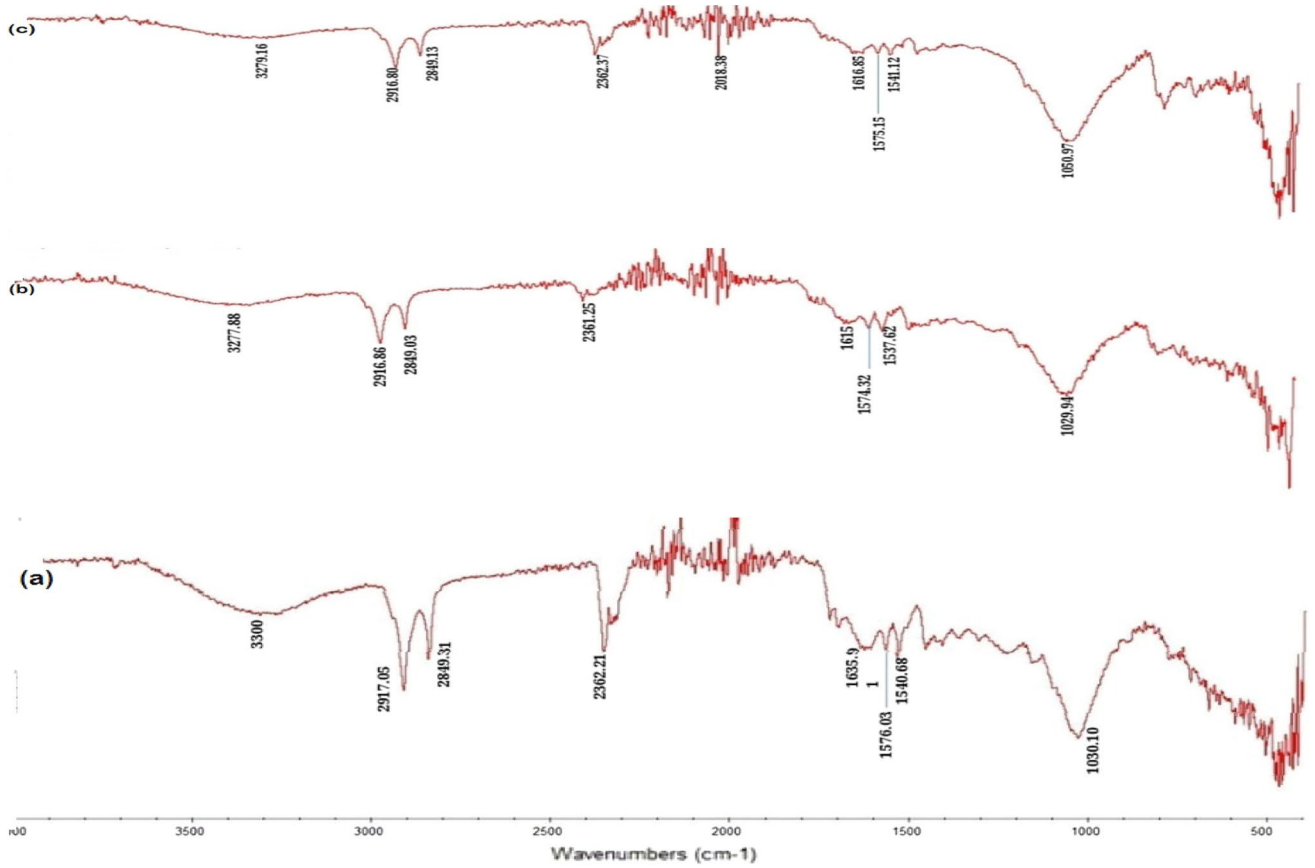

Fig. 3 FTIR spectra of fresh OP (**a**),Fe^{2+} ions adsorption on OP(**b**) Mn^{2+} ions adsorption on OP

Effect of initial concentration

Figure 8 shows that the removal percentage of Fe^{2+} and Mn^{2+} by using O.P and MSH decreases with the increase in initial concentration. For the adsorption of heavy metal ions, adequate sorption sites are needed at a lower metal ion initial concentration. However, at high concentrations, the available adsorption sites are reduced and the percentage of the reduction of heavy metals depends on the initial concentration (Funes et al. 2014)**.** The initial concentration analysis of Fe^{2+} and Mn^{2+} was investigated for each adsorbent with a pH value set at 5 in the range of 10–300 mg/L. For OP, the sorption percentage decreased from 93 and 90% to 34.16% and 32.5%, Fe^{2+} and Mn^{2+}, respectively. The percentage sorption reduction for MSH decreased from 98.5 to 97% for Fe^{2+} and Mn^{2+} to 33% and 37%, respectively.The improvement in the initial concentration of metal also increases the relationship of metal and adsorbent. Therefore, an increase in initial metal concentration increases metal adsorption absorption. This is due to the increase in the concentration gradient's motivating force with the increase in the original metal concentration (Kumar et al. 2010).

Effect of contact time

Figure 9 shows the adsorption data of Fe^{2+} and Mn^{2+} onto OP and MSH adsorbents at different time intervals. The experiments were carried out at different contact time 5 to 120 min using jar test apparatus at 100 rpm with adsorbent dosage 10 g, initial concentration 50 mg/l at a pH 5 and 500 ml contact solution. At the first 20 min, the relative elimination of Fe^{2+} and Mn^{2+} reaches to 58%, 46% onto OP and 65%, 49% onto MSH, respectively. The removal proceeded was at a slower pace for OP and MSH until 120 min. At the beginning, there were some empty active sites for adsorption, but the number reduction was achieved after the optimal time, since most of these sites were filled with ions (Kumar et al. 2010).

Adsorption isotherms

The values of K_F and 1/n can be expressed from the intercept and slope of Log q_e versus Log c_e (Fig. 10c and d). The n_F value in the Freundlich model represents the reactivity of biomass's active sites. According to (Bhatt et al. 2012), if a value of $n_F = 1$, the adsorption is linear, for $n_F < 1$, the

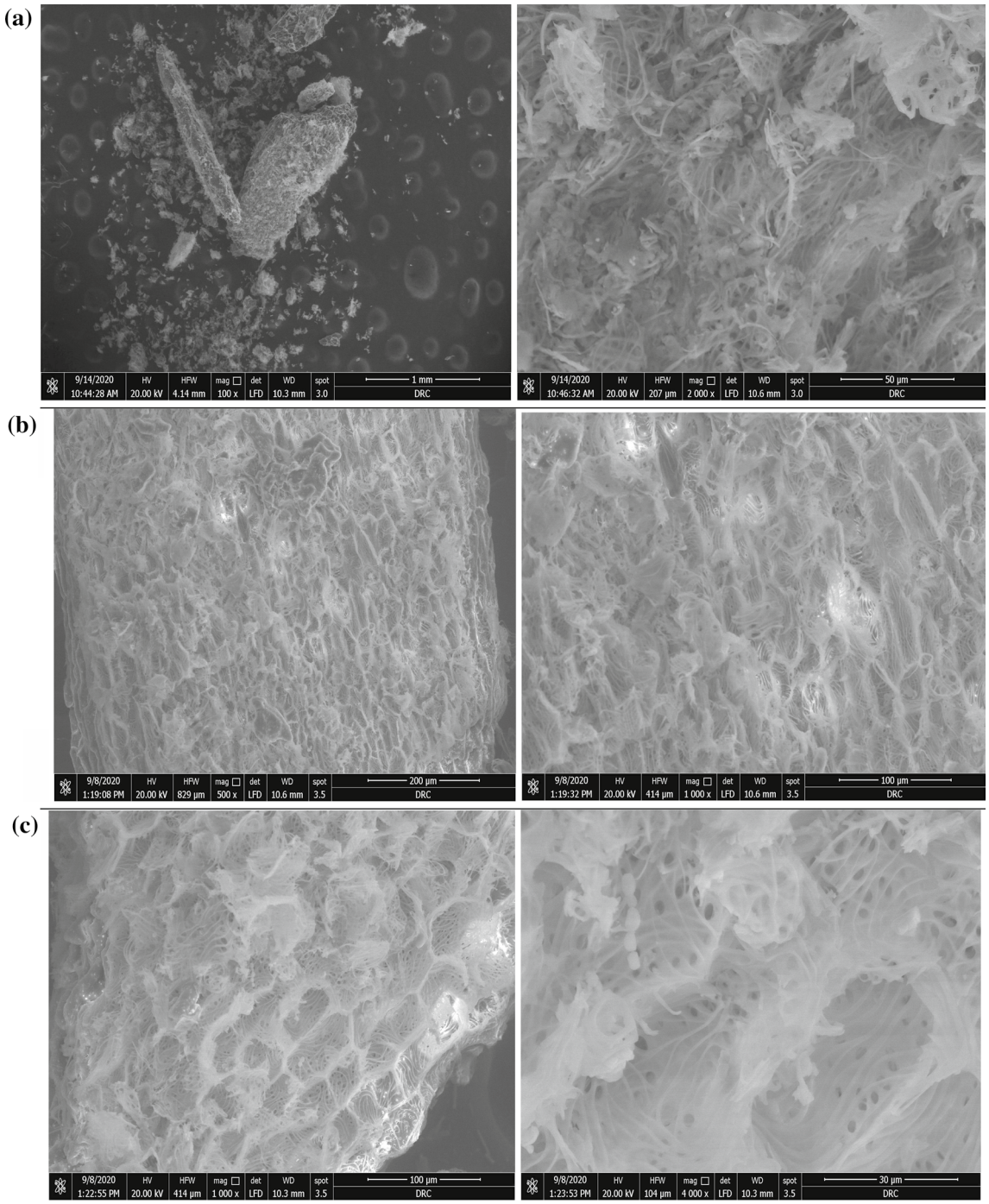

Fig. 4 SEM image of MSH before adsorption **a** MSH after Fe^{2+} adsorption **b** MSH after Mn^{2+} adsorption **c** at two magnifications

adsorption is chemisorption, and for $n_F > 1$ the adsorption is a favorable physical adsorption. From Table 1, it was found that n_F values are greater than unity and physical adsorption was shown favorable for adsorption of Fe and Mn on OP and MSH. The maximum adsorption capacity of OP and MSH adsorbents for the removal Fe and Mn ions is compared with other adsorbents reported in previous works, Table 2. The q_m calculated from the Langmuir model were determined to be 10.406 mg/g, 10.28 mg/g for $Fe2^{+}$on OP and MSH, respectively, and 10.460 mg/g, 11.641 mg/g for $Mn2^{+}$ on OP an MSH, respectively. It is clear that the data obtained for the adsorption of Fe^{2+} and Mn^{2+}on OP are well fitted to the Langmuir model, that indicates that Fe^{2+} and Mn^{2+}on OP and MSH are monolayer coverage(Tan et al. 2015).

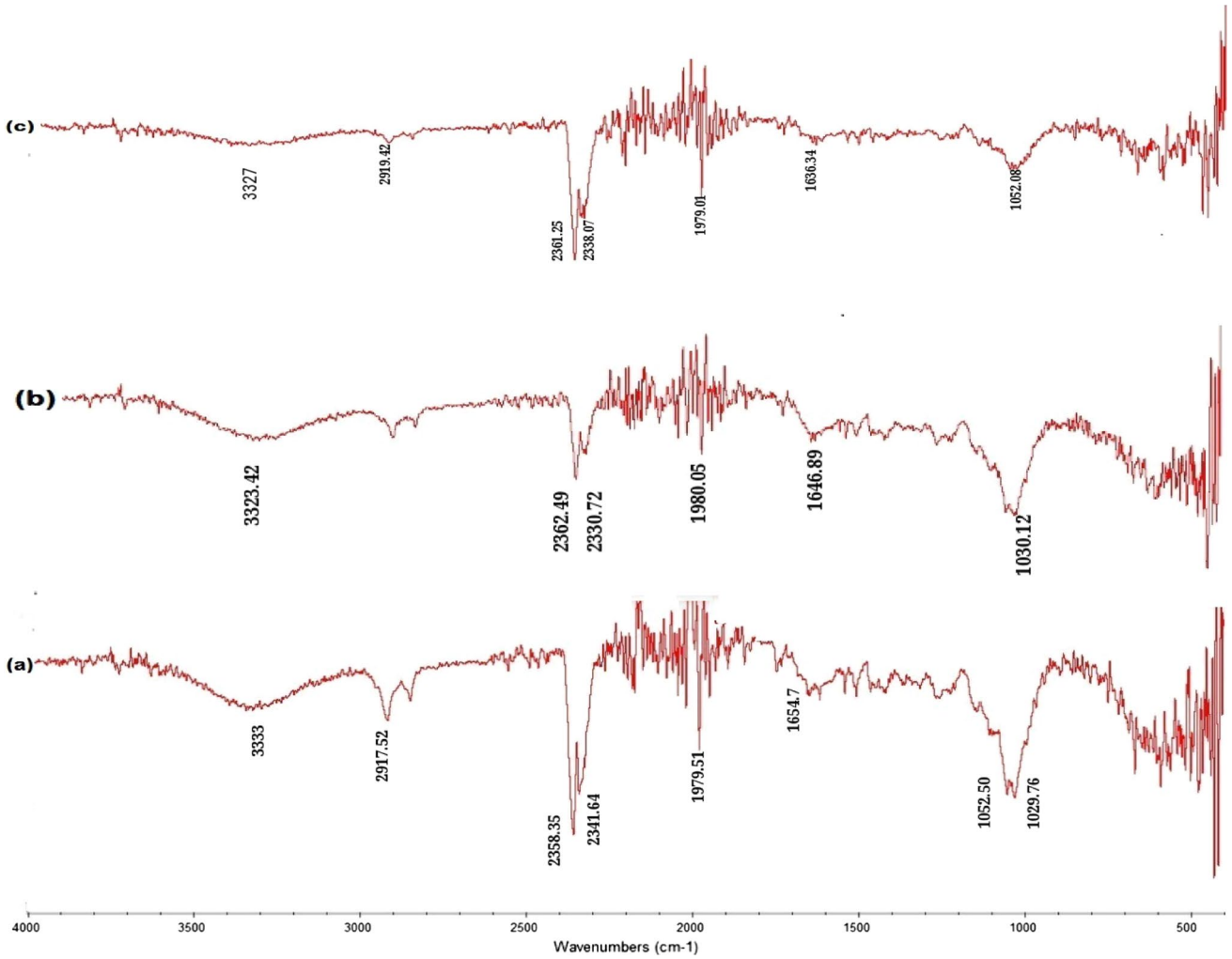

Fig. 5 FTIR spectra of fresh MSH (**a**), Fe^{2+} ions adsorption on MSH(**b**) Mn^{2+} ions adsorption on MSH

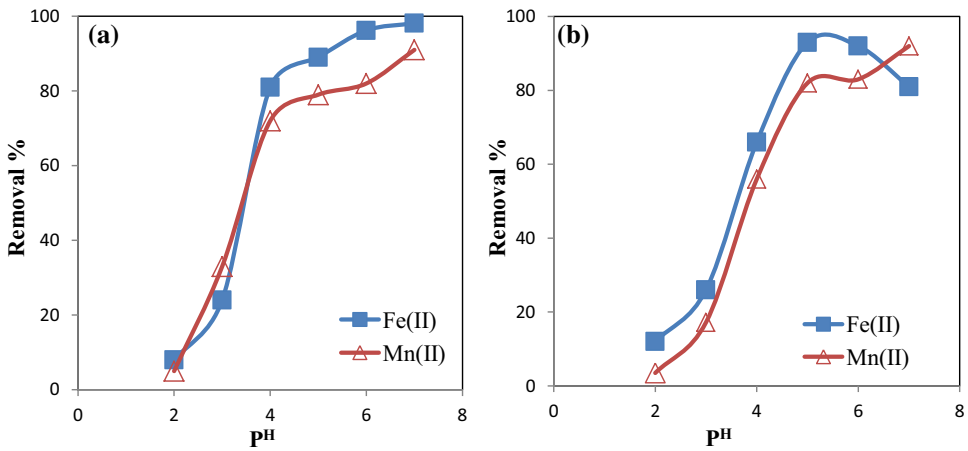

Fig. 6 Effect of pH on removal of of Fe^{2+} and Mn^{2+} using O.P adsorbent (**a**) and MSH adsorbent (**b**). Conditions, initial metal concentration, 50 mg/l, adsorbate solution volume 500 ml, adsorbent dose 10 g/l, contact time 120 min

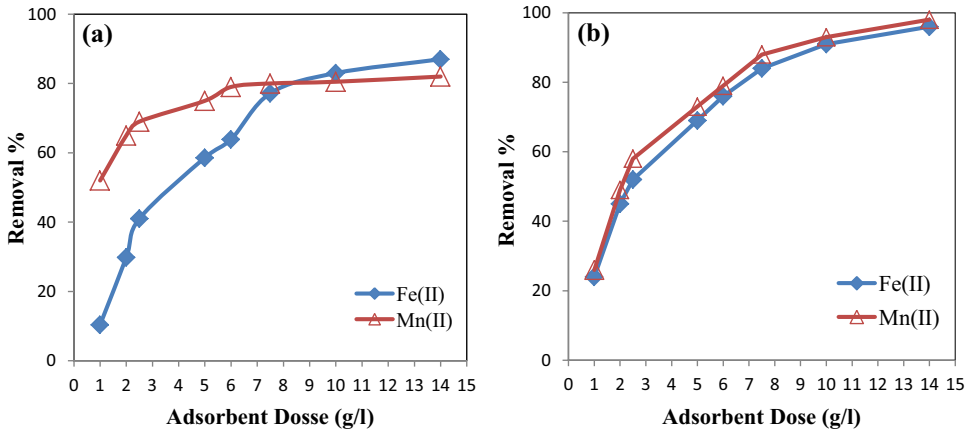

Figure. 7 Effect of adsorbent dose O.P (**a**) and MSH (**b**) Conditions, initial metal concentration, 50 mg/l, adsorbate solution volume 500 ml, pH 5, contact time 120 min

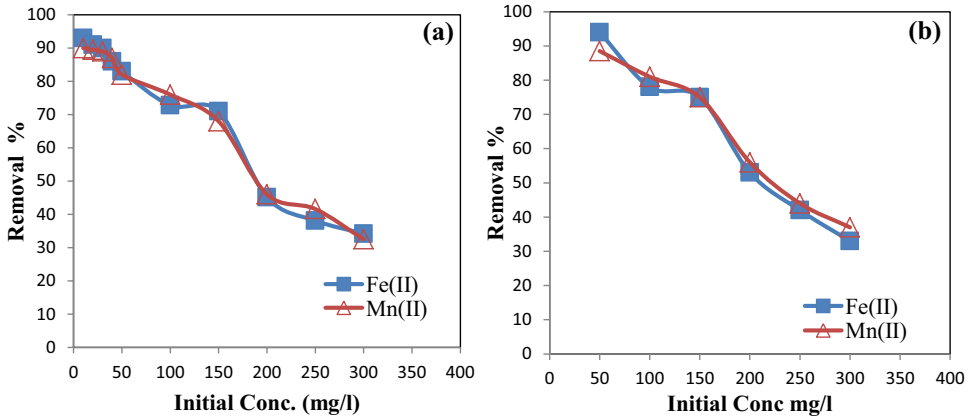

Fig. 8 Effect of initial concentration of Fe^{2+} and Mn^{2+} ions (mg /L) on removal of 500 ml onto 5 g for OP adsorbent (**a**) MSH adsorbent (**b**) at pH 5 for 120 min contact time

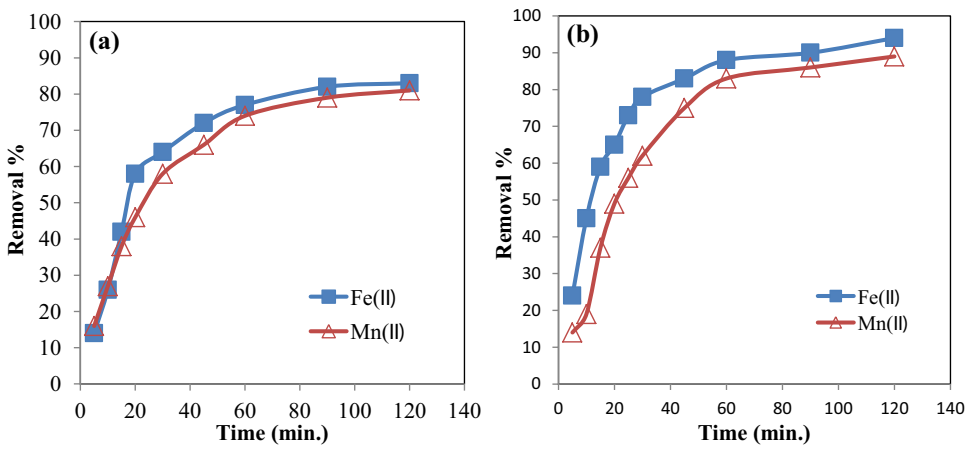

Fig. 9 Effect of contact time on removal Fe^{2+} and Mn^{2+} ions in (a) OP adsorbent (**a**) and MSH adsorbent (**b**).Conditions, initial metal concentration, 50 mg/l, dose 10 g/l, pH 5

Adsorption kinetics

Figure 11a and b showed the Kinetics models for $Fe^{2+}$and Mn^{2+} adsorption onto OP and MSH. From plotting log (q_e _ q_t) versus t, K_1 and q_e can be obtained from the slope and intercept, respectively. From Table 3, the correlation coefficients (R^2) for the pseudo-second-order kinetic model are higher than those for the pseudo-first-order kinetic model, and the q_e values calculated from the pseudo-second-order kinetic model are very close to the experimental ones. These results suggest that the overall rates of the adsorption of Fe^{2+}, Mn^{2+} onto OP and MSH are controlled by chemical adsorption.

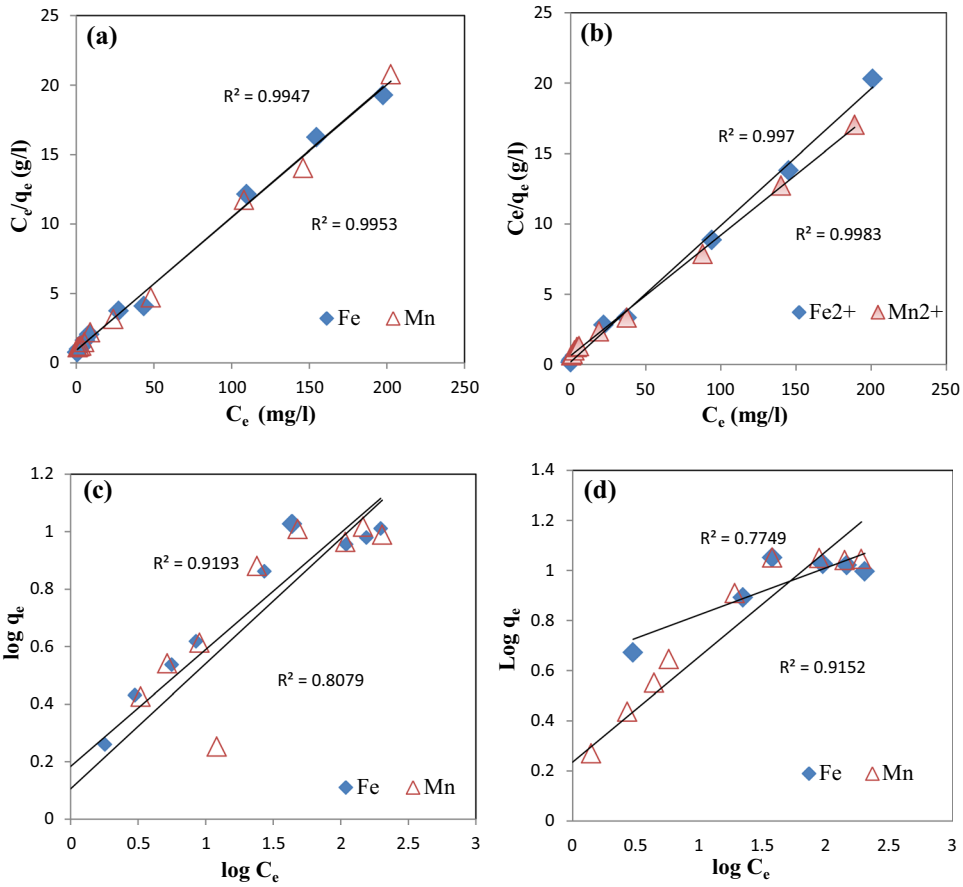

Fig. 10 Langmuir isotherm for the adsorption of Fe^{2+} and Mn^{2+} on OP (**a**), MSH (**b**) & Freundlich isotherm for the adsorption of Fe^{2+} and Mn^{2+} on OP (**c**), MSH (**d**)

Table 1 Parameters for the Langmuir and Freundlich models of $Fe^{2+}$and Mn^{2+} adsorption on OP and MSH adsorbent

Adsorbent	Metal ion	Langmauir			Freundlich		
		q_{max} (mg/g)	K_L (L/mg)	R^2	k_f	n	R^2
OP	Fe^{2+}	10.406	0.1074	0.9947	1.525	2.462	0.9193
	Mn^{2+}	10.460	0.1046	0.9953	1.276	2.297	0.8079
MSH	Fe^{2+}	10.28	0.5189	0.997	1	4.315	0.7749
	Mn^{2+}	11.641	0.1367	0.9983	11.641	2.37	0.9152

Table 2 Comparison of OP and MSH for the removal of Heavy Metals from aqueous solutions

Adsorbent	Metal ions	Condition	%, q	Reference
Moringa oleifera leaf	Mn^{2+}	contact time of 120 min, pH 6,dosage 0.2 g/l, c_o 5 mg/l	19.230	(Muthuraman 2017)
M. oleifera seeds	Fe(II)	c_o 5 mg/L contact time 60 min	41%	(Pramanik, Pramanik et al. 2016)
crude olive stones	Fe(II)	Dose 37.5 g dm − 3, c_o 20mgdm − 3, 117 rpm, size < 4.8 mm	1.2 mg/g	(Nieto et al. 2010)
(Moringa) Seed Pods	Fe Mn	contact time of 60 min pH 8, Co 20 mg/l, Dosage 1 g, Particle size 100 µm	Fe,80.9%Mn,100.0%	(Maina, Obuseng et al. 2016)
OP	Fe,Mn	Dose 5 g, 100 rpm,2 h pH 5 C_o 50 mg/l	10.406 10.460	This study
MSH	Fe,Mn		10.28 11.641	This study

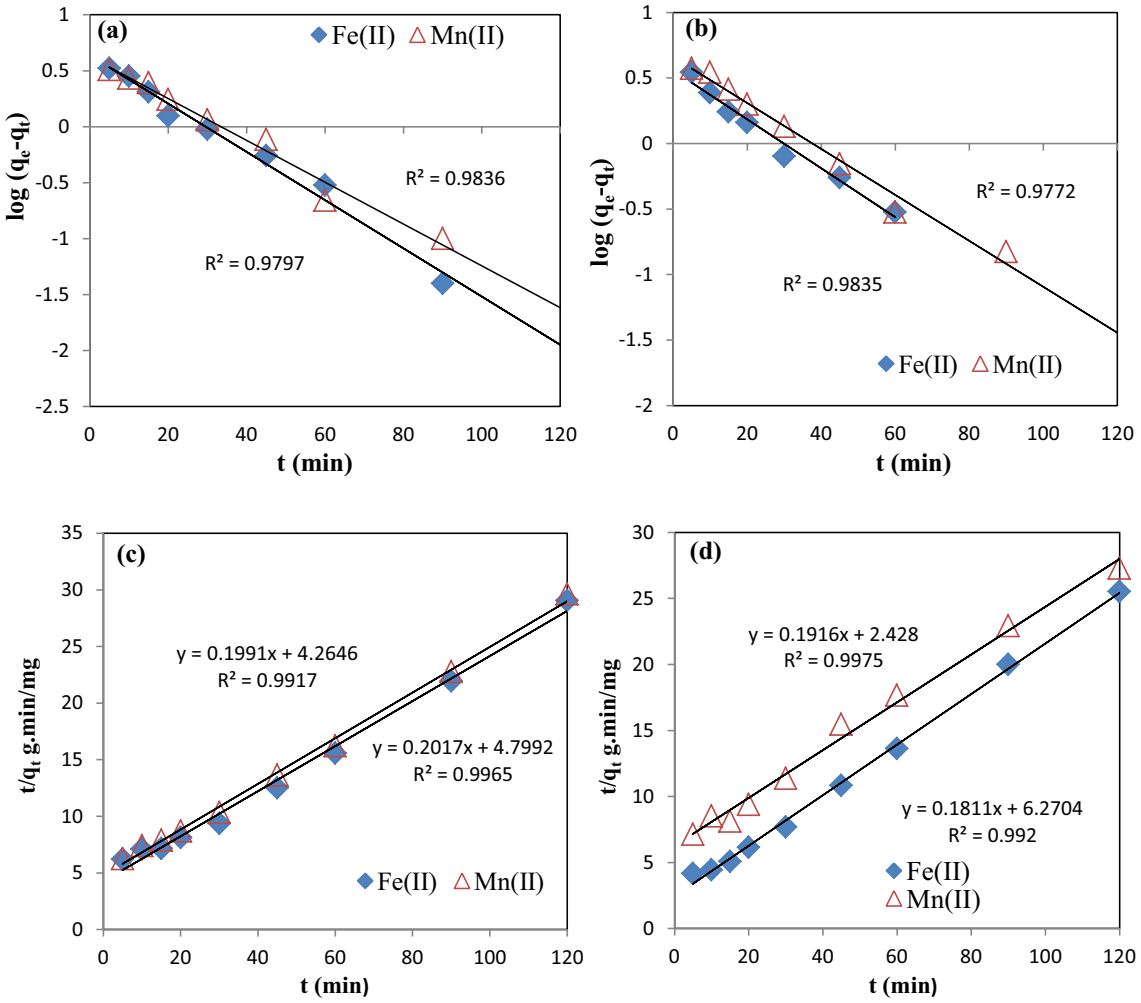

Fig. 11 Pseudo-first-order kinetic model for $Fe^{2+}$and Mn^{2+} adsorption onto OP (**a**) and MSH adsorbents (**b**) & Pseudo- second-order kinetic model for $Fe^{2+}$and Mn^{2+} adsorption onto OP (**c**) and MSH adsorbents (**d**)

Table 3 Parameters for the pseudo-first-order and pseudo -second-order models of Fe^{2+} and Mn^{2+} adsorption ions on O.P and MSH adsorbents

Adsorbent	Metal ion	Pseudo-first-order			Pseudo-second-order			
		q_e (cal) (mg/g)	K_1 (L/mg)	R^2	q_e (cal) (mg/g)	K_2 (g/mg min)	R^2	q_e (exp) (mg/g)
OP	Fe^{2+}	4.34	0.0497	0.9836	5.02	0.00936	0.9917	4.15
	Mn^{2+}	4.22	0.043	0.9797	4.96	0.00847	0.9965	4.1
MSH	Fe^{2+}	3.63	0.043	0.9772	5.2	0.006	0.9975	4.7
	Mn^{2+}	4.58	0.040	0.9835	5.52	0.005	0.992	4.42

Regeneration study

The percentage elimination of Fe^{2+} on OP and MSH (Fig. 12b) decreases by around 11% and 23%, respectively, after five cycles. And the percentage elimination of Mn^{2+} on OP and MSH (Fig. 12c) also falls by 16 and 29%, respectively. Desorption tests were conducted with and without washing using deionized H2O, 0.5 N HCl, 0.5 N NaOH, 0.02 N EDTA and the results are shown in the figure. The adsorbent's reusability was accomplished by washing with DI water. This discovery also indicates that one of the key pathways for the desorption process was ion exchange. However, washing the metal laden adsorbent with deionized water did not demonstrate any potential for desorption (Ngah and Hanafiah 2008). This decrease can be attributed to loss of binding sites after each desorption step (Zhang

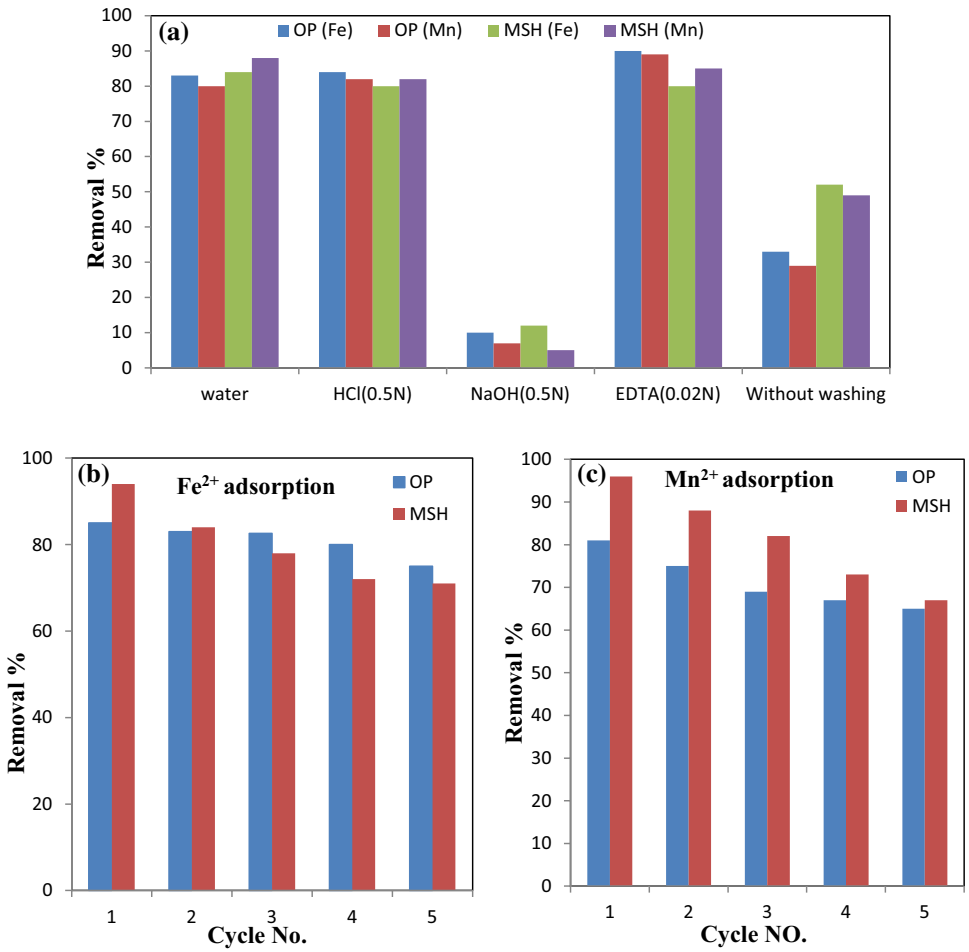

Fig. 12 Desorption studies of each OP and MSH adsorbents for Fe^{2+} and Mn^{2+} (**a**) & Reusability studies of OP and MSH adsorbents for Fe^{2+} adsorption (**b**), Mn^{2+} adsorption (**c**)

Table4 Use of moringa oleifera Seeds and olive pomace in the Removal of Iron and Manganese Ions from Aqueous Samples

SAMPLE	Adsorbent	Conc. Before mg/l		Conc. after mg/l	
		Fe	Mn	Fe	Mn
A	OP	6.96	0.819	0.557	0.074
	MSH	6.96	0.819	0.139	0.041
B	OP	5.39	0.9207	0.431	0.083
	MSH	5.39	0.9207	0.108	0.046

et al. 2011). The results showed that the used adsorbent materials could be reused as adsorbents following five cycles of adsorption/desorption with a small loss in its adsorption capacity in industrial applications.

Application

The studied adsorbent was applied in the adsorption of Fe^{2+} and Mn^{2+} ions from surface water sample (A) and underground sample(B) taken from the study area. The samples were subsequently treated with the two adsorbent materials to determine the percentage removal of the metal. The samples (500 mL) were then treated with 5 g of adsorbent at optimum pH 5 and optimum time of 120 min. The two metal ions were quantified using spectrophotometer before and after the removal experiments as shown in Table 4. The results showed that OP and MSH are effective in removing Fe^{2+} and Mn^{2+} from water samples. It was found that the removal percentage of Fe^{2+} and Mn^{2+} were 92%, 91% by using OP adsorbent and 98%, 95% by using MSH adsorbent, respectively.

Conclusion

In this work, the OP and MSH adsorbents were prepared and defined by FTIR and SEM to validate, respectively, the functional groups and the morphological structure. The results obtained showed an optimal adsorbent dosage of 10 g/l at a pH of 5 and a balance time of 120 min. The pseudo-second-order model was followed by the adsorption kinetics of Fe^{2+} and Mn^{2+} on OP and MSH, and the Langmuir model worked well with the adsorption isotherm. The overall adsorption power of the OP adsorbent for Fe^{2+} and Mn^{2+} was 10.406 and 10.460 mg/g, and the MSH was 10.28 and 11.641 mg/g

for Fe^{2+} and Mn^{2+}, respectively. At various concentrations, the equilibrium parameter (RL) was less than unity, suggesting that the adsorption of metal ions into adsorbents is favorable.

Author Contributions All authors contributed to the study conception and design. Material preparation, data collection and analysis were performed by [Ibrahim Hegazy], [Mohamed E.A. Ali], [Ehab H. Zaghlool] and [Ragaa Elsheikh]. The first draft of the manuscript was written by [Ibrahim Hegazy], and all authors commented on previous versions of the manuscript. All authors read and approved the final manuscript.

Funding No funding was received for this work.

Data Availability Data available on request from the authors.

Declarations

Conflicts of interest The authors declare that they have no conflict of interest.

References

Ali EN, Seng HT (2018) Heavy metals (Fe, Cu, and Cr) removal from wastewater by Moringa oleifera press cake. MATEC Web of Conferences, EDP Sciences

Aziz N, Jayasuriya N, Fan L (2016) Adsorption study on Moringa oleifera seeds and Musa cavendish as natural water purification agents for removal of lead, nickel and cadmium from drinking water. IOP Conference Series: Materials Science and Engineering, IOP Publishing.

Aziz N, Jayasuriya N, Fan L (2016) Adsorption study on Moringa oleifera seeds and Musa cavendish as natural water purification agents for removal of Lead, Nickel and Cadmium from drinking water. Mat Sci Eng 136:1–9

Bayramoğlu G, Çelik G, Arica MY (2006) Biosorption of reactive blue 4 dye by native and treated fungus Phanerocheate chrysosporium: batch and continuous flow system studies. J Hazard Mater 137(3):1689–1697

Bhatt AS, Sakaria PL, Vasudevan M, Pawar RR, Sudheesh N, Bajaj HC, Mody HM (2012) Adsorption of an anionic dye from aqueous medium by organoclays: equilibrium modeling, kinetic and thermodynamic exploration. RSC Adv 2(23):8663–8671

Blázquez G, Hernainz F, Calero M, Ruiz-Nunez L (2005) Removal of cadmium ions with olive stones: the effect of somes parameters. Process Biochem 40(8):2649–2654

Bouguerra W, Mnif A, Hamrouni B, Dhahbi M (2008) Boron removal by adsorption onto activated alumina and by reverse osmosis. Desalination 223(1–3):31–37

Cengeloglu Y, Tor A, Arslan G, Ersoz M, Gezgin S (2007) Removal of boron from aqueous solution by using neutralized red mud. J Hazard Mater 142(1–2):412–417

Demirbas E, Kobya M, Senturk E, Ozkan T (2004) Adsorption kinetics for the removal of chromium (VI) from aqueous solutions on the activated carbons prepared from agricultural wastes. Water Sa 30(4):533–539

Elouear Z, Bouzid J, Boujelben N, Amor RB (2009) Study of adsorbent derived from exhausted olive pomace for the removal of Pb2+ and Zn2+ from aqueous solutions. Environ Eng Sci 26(4):767–774

Fiol N, Villaescusa I, Martínez M, Miralles N, Poch J, Serarols J (2006) Sorption of Pb (II), Ni (II), Cu (II) and Cd (II) from aqueous solution by olive stone waste. Sep Purif Technol 50(1):132–140

Freundlich H (1906) Over the adsorption in solution. J Phys Chem 57(385471):1100–1107

Funes A, De Vicente J, Cruz-Pizarro L, De Vicente I (2014) The influence of pH on manganese removal by magnetic microparticles in solution. Water Res 53:110–122

Ghafar F, Mohtar A, Sapawe N, Hadi NH, Salleh MRM (2017) Chemically modified Moringa oleifera seed husks as low cost adsorbent for removal of copper from aqueous solution. AIP Conference Proceedings, AIP Publishing LLC

Gharaibeh S, AbuEl-Sha-r W, Al-Kofahi M (1999) Removal of selected heavy metals from aqueous solutions using a solid by-product from the Jordanian oil shale refining. Environ Geol 39(2):113–116

Hawari A, Khraisheh M, Al-Ghouti MA (2014) Characteristics of olive mill solid residue and its application in remediation of Pb2+, Cu2+ and Ni2+ from aqueous solution: Mechanistic study. Chem Eng J 251:329–336

Ince M, Ince OK (2017) An overview of adsorption technique for heavy metal removal from water/wastewater: a critical review. Int J Pure Appl Sci 3(2):10–19

Kumar PS, Vincent C, Kirthika K, Kumar KS (2010) Kinetics and equilibrium studies of Pb2+ in removal from aqueous solutions by use of nano-silversol-coated activated carbon. Braz J Chem Eng 27(2):339–346

Lagergren S (1898) "Zur theorie der sogenannten adsorption geloster stoffe"

Langmuir I (1918) The adsorption of gases on plane surfaces of glass, mica and platinum. J Am Chem Soc 40(9):1361–1403

Maina IW, Obuseng V, Nareetsile F (2016) Use of Moringa oleifera (Moringa) seed pods and Sclerocarya birrea (Morula) nut shells for removal of heavy metals from wastewater and borehole water. J Chem 2016

Martín-Lara M, Hernáinz F, Calero M, Blázquez G, Tenorio G (2009) Surface chemistry evaluation of some solid wastes from olive-oil industry used for lead removal from aqueous solutions. Biochem Eng J 44(2–3):151–159

Martín-Lara M, Pagnanelli F, Mainelli S, Calero M, Toro L (2008) Chemical treatment of olive pomace: Effect on acid-basic properties and metal biosorption capacity. J Hazard Mater 156(1–3):448–457

Ngah WW, Hanafiah M (2008) Biosorption of copper ions from dilute aqueous solutions on base treatedrubber (Hevea brasiliensis) leaves powder: kinetics, isotherm, and biosorption mechanisms. J Environ Sci 20(10):1168–1176

Nieto LM, Alami SBD, Hodaifa G, Faur C, Rodríguez S, Giménez JA, Ochando J (2010) Adsorption of iron on crude olive stones. Ind Crops Prod 32(3):467–471

Ongulu RA (2015) Biosorption of Pb2+ and Cr2+ using Moringa oleifera and their adsorption isotherms

Ponnusami V, Krithika V, Madhuram R, Srivastava S (2007) Biosorption of reactive dye using acid-treated rice husk: factorial design analysis. J Hazard Mater, 142(1–2): 397 403

Rahman MS, Islam MR (2009) Effects of pH on isotherms modeling for Cu (II) ions adsorption using maple wood sawdust. Chem Eng J 149(1–3):273–280

Sadegh H, Mazloumbilandi M, Chahardouri M (2017) Low-cost materials with adsorption performance. Handbook of ecomaterials: 1-33

Saviozzi A, Levi-Minzi R, Cardelli R, Biasci A, Riffaldi R (2001) Suitability of moist olive pomace as soil amendment. Water Air Soil Pollut 128(1–2):13–22

Tan P, Sun J, Hu Y, Fang Z, Bi Q, Chen Y, Cheng J (2015) Adsorption of Cu2+, Cd2+ and Ni2+ from aqueous single metal solutions on graphene oxide membranes. J Hazard Mater 297:251–260

Tsai W-T, Hsu H-C, Su T-Y, Lin K-Y, Lin C-M (2008) Removal of basic dye (methylene blue) from wastewaters utilizing beer brewery waste. J Hazard Mater 154(1–3):73–78

Veglio F, Beolchini F (1997) Removal of metals by biosorption: a review. Hydrometallurgy 44(3):301–316

Volesky B (2001) Detoxification of metal-bearing effluents: biosorption for the next century. Hydrometallurgy 59(2–3):203–216

Ys H, Mckay G, Ys H, Mckay G (1999) Pseudo-second order model for sorption processes. Process Biochem 34(5):451–465

Zhang N, Qiu H, Si Y, Wang W, Gao J (2011) Fabrication of highly porous biodegradable monoliths strengthened by graphene oxide and their adsorption of metal ions. Carbon 49(3):827–837